

Auto-correlative weak-value amplification under strong noise background

Jing-Hui Huang^{1,4,*}, Xiang-Yun Hu^{1,4,†}, Xue-Ying Duan^{2,3}, Fei-Fan He¹, Huan Chen⁵, Jian-Qi An^{2,3}, and Guang-Jun Wang^{2,3}

¹*Institute of Geophysics and Geomatics, China University of Geosciences, Lumo Road 388, 430074 Wuhan, China.*

²*School of Automation, China University of Geosciences, Lumo Road 388, 430074 Wuhan, China.*

³*Hubei Key Laboratory of Advanced Control and Intelligent Automation for Complex Systems, Lumo Road 388, 430074 Wuhan, China.*

⁴*Engineering Research Center of Intelligent Technology for Geo-Exploration, Ministry of Education, China and*

⁵*School of Mathematics and Physics, China University of Geosciences, Lumo Road 388, 430074 Wuhan, China.*

In the general optical metro-logical protocols based on the weak-value amplification(WVA) approach, it is beneficial to choose the pre-selected state and the post-selected one to be nearly orthogonal for improving the sensitivity. However, the orthogonality of the post-selection decreases the probability of detecting photons and makes the weak measurement difficult, especially when there is strong noise background and the pointer is drowned in noise. In this article, we investigate a modified weak measurement protocol with a temporal pointer, namely, the auto-correlative weak-value amplification (AWVA) approach. We find it can significantly improve the precision of optical metrology under Gaussian white noise, especially with a negative signal-to-noise ratio. With the AWVA approach, a small longitudinal time delay (tiny phase shift) τ of a Gaussian pulse is measured by implementing two auto-correlative weak measurements. The small quantities are obtained by measuring the auto-correlation coefficient of the pulses instead of fitting the shift of the mean value of the probe. Simulation results show that the AWVA approach outperforms the standard WVA technique in the time domain, remarkably increasing the precision of weak measurement under strong noise background.

I. INTRODUCTION

Higher precision in the measurement of various quantities is a persistent goal of scientific communities. It is well known that the pre- and post-selection of the measured system have played a crucial role in amplifying detector signals in a weak measurement. The concept of the pre- and post-selection [1] originated from the work of Aharonov, Albert, and Vaidman in 1988. Theoretically, they found the measuring result of the component of a particle spin, called "the weak value", can be amplified by a large number, which opened up a gate for the quantum metrology [2–8] with the weak-value amplification (WVA).

Chronologically, a standard weak measurement includes an initial preparation of the measured system(pre-selection), weak coupling between the system and the pointer, a post-selection of the system, and a projecting measurement on the pointer to read out the results [9]. For now, the widely used pointers in weak measurement are the shifts of mean values, such as the temporal shifts [10–13], the momentum shifts [14, 15], the frequency shifts [16, 17], and even the angular rotation shifts [18, 19]. But even so, the WVA scheme entails an inherent dilemma: when the pre- and post-selection are nearly orthogonal to achieve higher sensitivity, the probability of a successful post-selection will be reduced greatly [20, 21]. To obtain the observable distribution function, the times of repeated measurement

should be large and the requirements on the apparatus are strict [22]. For example, the resolution of the apparatus should be high enough and the intensity of the light source ought to be sufficiently strong.

Meanwhile, the determination of the pointer shift would inevitably be influenced by technique noise and the surrounding environment. Numerous studies [20, 21, 23] have been done to investigate the advantage of WVA in presence of noise. In particular, Knee et al. [21] argued that the amplified displacement offered no fundamental metrological advantage, due to the necessarily reduced probability of success. Using statistically rigorous arguments, Christopher et al. [20] showed that the technique of WVA does not perform better than standard statistical techniques for single parameter estimation or signal detection. Considering the measured system cannot be completely isolated from the surrounding environment and the instability of the element itself, the determination of the pointer shift will inevitably be influenced by many sources [23]: instability of the light source's spectrum and intensity, interference in the light path, thermal noise and shot noise of the detection, and other noise sources. A natural thought is to equate these noises with Gaussian white noises. In addition, Gaussian white noise has been replaced by colored noise (non-Gaussian) [24–27] in a variety of areas of physics, such as quantum Brownian motion in a general environment with non-local dissipation and colored noise [25], non-Gaussian noise-enhanced stability of foraging colony system [26]. The statistical properties of colored noise depend on the choice of the quantum state of the gravitational field [28]. However, in this paper, we assume that the contribution of all noise is Gaussian white noise and investigate the

* Email:jinghuihuang@cug.edu.cn

† Email:xyhu@cug.edu.cn

weak-value amplification technique under strong Gaussian white noise background.

It is encouraging that the WVA scheme based on the imaginary weak-value (in the frequency domain) has sound potential to outperform the standard measurement in presence of technical noise [10, 29–33]. There-into, Brunner et al. [10] proposed that the WVA scheme using the imaginary weak value amplification can result in 3 orders of magnitude higher precision than the traditional interference method. Therefore, the WVA scheme based on the imaginary weak value is currently used in the field of biosensors, such as a new chiral sensor based on weak measurement for estimation of a trace amount of chiral molecule [34], a tunable and high-sensitivity temperature-sensing method via WVA of Goos–änchen (GH) shifts in a graphene-coated system [35], even an optical system based on optical rotation via weak measurement for detection of single- and double-strand state of DNA [36]. Furthermore, there have been several optimization schemes to improve the WVA scheme based on analysis of its Fisher information [23, 32, 37, 38].

Note that so far how to achieve higher precision based on the WVA scheme with the temporal pointer (in the time domain) is seldom investigated, especially under strong noise background (corresponding to the negative SNR). Nevertheless, when the quality estimation is not measured in the context of rigorous experiments, different effects in the environment will inevitably cause signal noises, which makes the measurement with the WVA more difficult. Thus, further study of the WVA under noise is imperative. In this paper, we proposed a modified weak measurement protocol with a temporal pointer, namely, auto-correlative weak-value amplification (AWVA). It is motivated by the widely used auto-correlation technique for signal denoising in engineering [39–41], where auto-correlation is a signal processing method describing the correlation of a signal with a delayed copy of itself [40]. The AWVA technique can realize the WVA scheme under strong noise background. In particular, the measurements with Gaussian white noises are studied at a certain signal-to-noise ratio (SNR). By simulating these measurements on Simulink and Matlab, we show that the measurement with AWVA is superior to the measurement with WVA under strong noise background.

The paper is organized as follows. In Sec II.A, we briefly review the standard WVA technique for measuring a time delay τ , which is served as the coupling strength in WVA. In Sec II.B, we derive the AWVA technique for the time delay τ measurement and introduce the auto-correlative intensity Θ (units of voltage) to evaluate the weak value. In Sec III, we present both the WVA scheme and the AWVA scheme under the Gaussian white noises. In Sec IV, we show the analytic results with various types of noises and various coupling strengths. And Sec V is devoted to a summary and discussions.

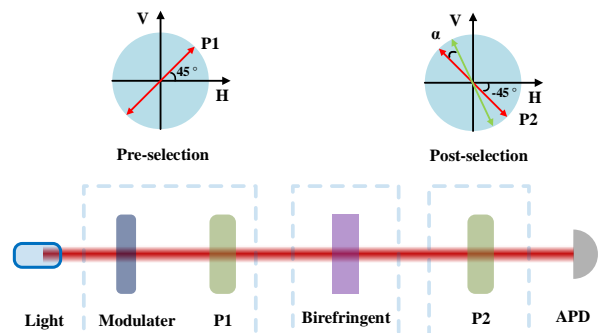


FIG. 1. Scheme of the standard WVA technique. The Gaussian beam is produced by the Light and Modulator. Then photons are pre-selected by the Polarizer 1 (P1) with the optical axis set at 45° . A time delay τ (corresponding to a phase shift between the horizontal polarized state $|H\rangle$ and vertical polarized state $|V\rangle$) is induced by a birefringent crystal (Birefringent). Finally, the photons are post-selected by the Polarizer 2 (P2) with an optical axis set at $\alpha - 45^\circ$, and the arrival time of single photons is measured with an avalanche photodiode (APD).

II. THEORY

A. The standard WVA technique

Let us briefly review the standard WVA technique of Ref. [10] with a two-level system in a quantum state $|\Phi\rangle$ and a measurement device represented by a temporal pointer $|\Psi\rangle$ to estimate a time delay. The scheme is shown in Fig. 1. First, the system is pre-selected into a polarized state

$$|\Phi_i\rangle = \sin\left(\frac{\pi}{4}\right)|H\rangle + \cos\left(\frac{\pi}{4}\right)|V\rangle = \frac{1}{\sqrt{2}}(|H\rangle + |V\rangle), \quad (1)$$

where $|H\rangle$ and $|V\rangle$ represent the horizontal and vertical polarized states respectively. Thus, the initial joint state of the system and the pointer is given by

$$|\Phi_i\rangle \otimes |\Psi_i\rangle = \frac{1}{\sqrt{2}}(|H\rangle + |V\rangle) |\Psi_i\rangle, \quad (2)$$

Then, the system and the pointer are weakly coupled with the interaction Hamiltonian $\hat{H} = \tau \hat{A} \otimes \hat{p}$, where the observable operator $\hat{A} = |H\rangle\langle H| - |V\rangle\langle V|$ and \hat{p} is the momentum operator conjugated to the position operator \hat{q} . In the regime of weak measurement, the time shift τ is much smaller than the pointer spread σ , and the final state of the pointer is given by:

$$\begin{aligned} |\Psi_f\rangle &= \langle \Phi_f | e^{-i\tau \hat{A} \otimes \hat{p}} | \Psi_i \rangle | \Phi_i \rangle \\ &\approx \langle \Phi_f | \left[1 - i\tau \hat{A} \otimes \hat{p} \right] | \Psi_i \rangle | \Phi_i \rangle \\ &= \langle \Phi_f | \Phi_i \rangle [1 - i\tau A_w \hat{p}] | \Psi_i \rangle \\ &= \langle \Phi_f | \Phi_i \rangle e^{-i\tau A_w \hat{p}} | \Psi_i \rangle, \end{aligned} \quad (3)$$

where $A_w := \langle \Phi_f | \hat{A} | \Phi_i \rangle / \langle \Phi_f | \Phi_i \rangle$ is the so-called weak value [1], represents the mean value of observable \hat{A} . Note that the time shift τ can be amplified by the weak value A_w . Normally, the weak value A_w is a complex number [42], thus the difference between the pointer in momentum space and that in position (temporal) space is used to perform the standard WVA. In particular, the imaginary part of A_w is associated with a shift of the pointer in momentum space, while the time shift τ in the position of the pointer is amplified by the real part of A_w [43]:

$$\Delta \langle \hat{q} \rangle = \frac{\int dq q |\langle q | \Psi_f \rangle|^2}{\int dq |\langle q | \Psi_f \rangle|^2} = \tau \text{Re}[A_w]. \quad (4)$$

In this paper, we design the weak measurement in the time domain and prepare the initial pointer with the Gaussian profile:

$$I_1^{in}(t; \tau) = |\langle q | \Psi_i \rangle|^2 = I_0 \frac{1}{(2\pi\omega^2)^{1/4}} e^{-(t-t_0)^2/4\omega^2}. \quad (5)$$

where I_0 represents the normalized factor. In order to amplify the ultra-small time shift τ , the system is post-selected into the state:

$$|\Phi_f\rangle = \sin(-\frac{\pi}{4} + \alpha) |H\rangle + \cos(-\frac{\pi}{4} + \alpha) |V\rangle, \quad (6)$$

where α should not be chosen as $\alpha=0$ to obtain non-vanishing probability of post-selection. One then obtain the weak value as:

$$A_w = \frac{\sin(-\frac{\pi}{4} + \alpha) - \cos(\frac{\pi}{4} + \alpha)}{\sin(-\frac{\pi}{4} + \alpha) + \cos(\frac{\pi}{4} + \alpha)} = -\cot\alpha, \quad (7)$$

The corresponding time shift τ can be obtained from the peak shift $\delta t = |\tau \text{Re}[A_w]| = \tau \cot\alpha$ of the signal detected by an avalanche photodiode (APD), with the detected signal I_1^{out} calculated from Eq. (3) as:

$$\begin{aligned} I_1^{out}(t; \tau) &= |\langle \Phi_f | \Phi_i \rangle|^2 e^{-2i\tau A_w \hat{p}} |\langle q | \Psi_i \rangle|^2 \\ &\approx I_0 \frac{(\sin\alpha)^2}{(2\pi\omega^2)^{1/4}} e^{-(t-t_0-\delta t)^2/4\omega^2} \end{aligned} \quad (8)$$

In principle, a larger peak shift δt as well as the weak value are obtained by choosing a smaller α , at a cost of decreasing the probability of post-selection $\mathcal{P} = |\langle \Phi_f | \Phi_i \rangle|^2 = (\sin\alpha)^2$. Note that the low probability \mathcal{P} leads to a weak signal and makes the weak measurement more difficult under strong noise background. In the next subsection, we will improve it with an AWVA technique.

B. AWVA technique with auto-correlative intensity

We display the scheme of the AWVA technique in Fig. 2, in which we introduce an auto-correlative intensity Θ for estimating the time shift τ introduced by the

birefringent crystal. The main difference between the two schemes is that an additional light path is added in the AWVA scheme, by dividing the light after pre-selection into two light paths with a beam splitter (BS, splitting ratio 50:50). In one path, light passes through the birefringent crystal and P2 as in the WVA scheme, while in the other path light passes only through Polarizer 3 (P3) for an auto-correlative measurement.

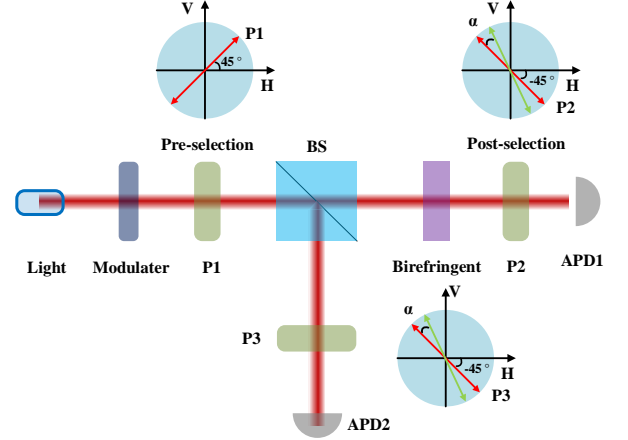


FIG. 2. Scheme of the AWVA technique. The light path is similar to that in the WVA scheme (Fig. 1), except for a 50:50 beam splitter being inserted between P1 and Birefringent to add a light path for an auto-correlative measurement. The optical axis of Polarizer 3 (P3) is also set at $\alpha - 45^\circ$.

The signal $I_{21}^{out}(t)$ detected at APD1 is similar to Eq.8 except the intensity being halved by the BS

$$I_{21}^{out}(t; \tau) = \frac{I_0}{2} \frac{(\sin\alpha)^2}{(2\pi\omega^2)^{1/4}} e^{-(t-t_0-\delta t)^2/4\omega^2} \quad (9)$$

Considering the light only passing through P3, there is no shift of the mean value of the pointer and the signal $I_{22}^{out}(t; \tau)$ detected at APD2 is given as:

$$I_{22}^{out}(t; \tau) = \frac{I_0}{2} \frac{(\sin\alpha)^2}{(2\pi\omega^2)^{1/4}} e^{-(t-t_0)^2/4\omega^2}. \quad (10)$$

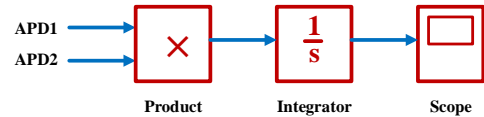


FIG. 3. Scheme of the signal processing module with AWVA technique.

In this paper, we introduce the new quantity Θ to estimate the time shift τ rather than the peak shift of the pointer. Θ is measured with the scheme shown in Fig. 3. The signals $I_{21}^{out}(t; \tau)$ and $I_{22}^{out}(t; \tau)$ detected at APD1 and APD2 pass through the "Product" and the "Integrator". Finally, the Scope detects the " Θ " signal, which

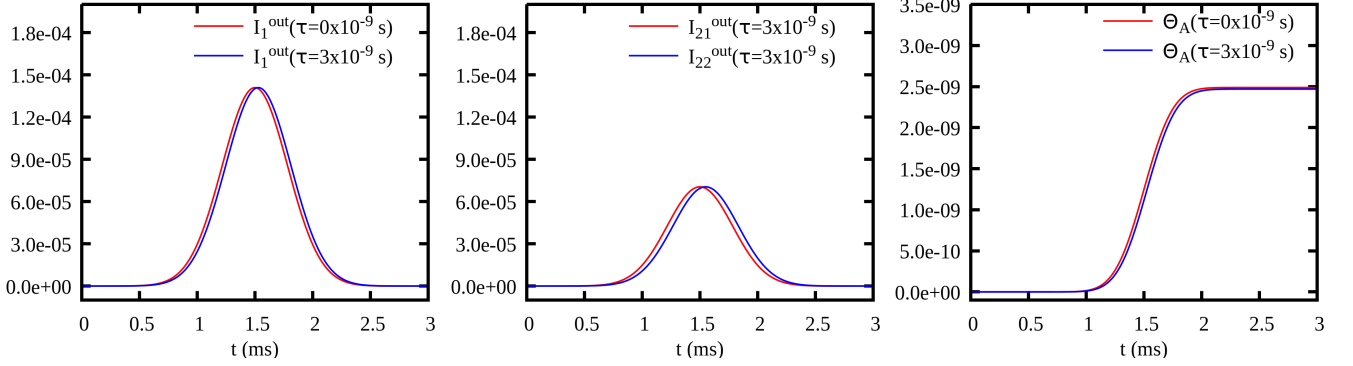


FIG. 4. Simulation results with WVA and AWVA schemes in absence of noises. Left panels: the signals $I_1^{out}(t; \tau)$ with $\tau = 0 \times 10^{-9}$ s and $\tau = 3 \times 10^{-9}$ s in the WVA scheme. Middle panels: the signals $I_{21}^{out}(t; \tau)$ as well as $I_{22}^{out}(t; \tau)$ with $\tau = 3 \times 10^{-9}$ s in the AWVA scheme. Right panels: the signals I_A^{AC} with $\tau = 0 \times 10^{-9}$ s and $\tau = 3 \times 10^{-9}$ s in the AWVA scheme. The units of the qualities $I_{21}^{out}(t; \tau)$, $I_{22}^{out}(t; \tau)$ and $I_{22}^{out}(t; \tau)$ are units of I_0 , the quality I_A^{AC} is units of voltage.

is mathematically given as:

$$\Theta_A(t; \tau) = \int_0^t I_{21}^{out}(t; \tau) \times I_{22}^{out}(t) dt \quad (11)$$

$$= \frac{I_0^2 (\sin \alpha)^4}{4 (2\pi\omega^2)^{1/8}} \int_0^t e^{-[(t-t_0)^2 + (t-t_0-\delta t)^2]/4\omega^2} dt.$$

The numerical results in absence of noises in the WVA scheme and the AWVA scheme are displayed in Fig. 4. In the WVA scheme, the time shift τ can be estimated by fitting the Gaussian signals $I_1^{out}(\tau = 0 \times 10^{-9} s)$ and $I_1^{out}(\tau = 3 \times 10^{-9} s)$. In the AWVA scheme, the time shift τ is estimated with the values of Θ . Eq. (11) also indicates that the value of $\Theta_A(t; \tau)$ depends strongly on the integral time t , which affects the sensitivity of the measurement with the AWVA technique. We will show and discuss the results in the next section.

The signal processing module shown in Fig. 3 can be implemented by both digital circuits and analog circuits. However, in this paper, we will only simulate the signal processing process in Simulink and MATLAB. The tools in Simulink allow us to implement weak measurements under various types of noise, and these simulation results will be shown in the following part.

III. WVA AND AWVA UNDER GAUSSIAN WHITE NOISES

It has been pointed out that technique noise [20, 21, 23] has a great influence on the weak measurement. To simulate the WVA and AWVA schemes with the temporal pointer on Simulink in a realistic situation, the effects of Gaussian white noises with different SNR on the two schemes are investigated firstly.

In this paper, we approximately simplified light noise from the instability of the light source, interference in the light path, thermal noise and shot noise of the detection and noises from other unknown sources as Gaussian noise. The characteristic of Gaussian white noise is

that its power spectral density and the fast Fourier transform (FFT) result are uniformly distributed. Especially, the Gaussian normal distribution denoted as $\mathbf{N}(t, \sigma^2, \xi)$ is generated by the pseudo-random number generator in Simulink, where σ^2 is the variance of the random signal. ξ is the random seed and represents the initial value used to generate a pseudo-random number in Simulink. The noise $\mathbf{N}(t, \sigma^2, \xi)$ with different ξ is corresponding to the results of multiple measurements (different times). Note that thermal noise and shot noise of the detection may cause the different series of noises detected on APD1 and APD2. In addition, the influence of the noise of different time series is also investigated in Section IV E.

The Gaussian white noise $\mathbf{N}(t, \sigma^2 = 1.0 \times 10^{-5}, \xi = 0)$, the power spectral density $\mathbf{PSD}(f, \sigma^2 = 1.0 \times 10^{-5}, \xi = 0)$ and the corresponding $\mathbf{FFT}(f, \sigma^2 = 1.0 \times 10^{-5}, \xi = 0)$ results are shown in Fig. 5. Note that Gaussian white noise is not only uncorrelated but also statistically independent between random variables at two different moments. Thus, on the basis of auto-correlation technique for signal denoising in engineering [39–41], the $\Theta_{NN}(t; \tau)$ of the Gaussian white noise $\mathbf{N}(t, \sigma^2)$ is defined as:

$$\Theta_{NN}(t; \tau) = \int_0^t \mathbf{N}(t, \sigma^2, \xi; \tau) \times \mathbf{N}(t, \sigma^2, \xi; \tau) dt$$

$$= 0(t \rightarrow \infty). \quad (12)$$

Then, we add the noise $\mathbf{N}(t, \sigma^2, \xi; \tau)$ into both the WVA scheme and the AWVA scheme. For the measurement with the WVA technique, one get the final signal $I_{1+N}^{out}(t; \tau)$ under $\mathbf{N}(t, \sigma^2)$ as:

$$I_{1+N}^{out}(t; \tau) = I_1^{out}(t; \tau) + \mathbf{N}(t, \sigma^2). \quad (13)$$

Now we need to evaluate the mean shift δt by the Gaussian fitting the result of $I_{1+N}^{out}(t; \tau; N)$. Obviously, the noise $\mathbf{N}(t, \sigma^2, \xi)$ will lead to an uncertainty of estimating δt . The simulation results with different simulation conditions are shown in Fig. 8, Table. I and Table. III.

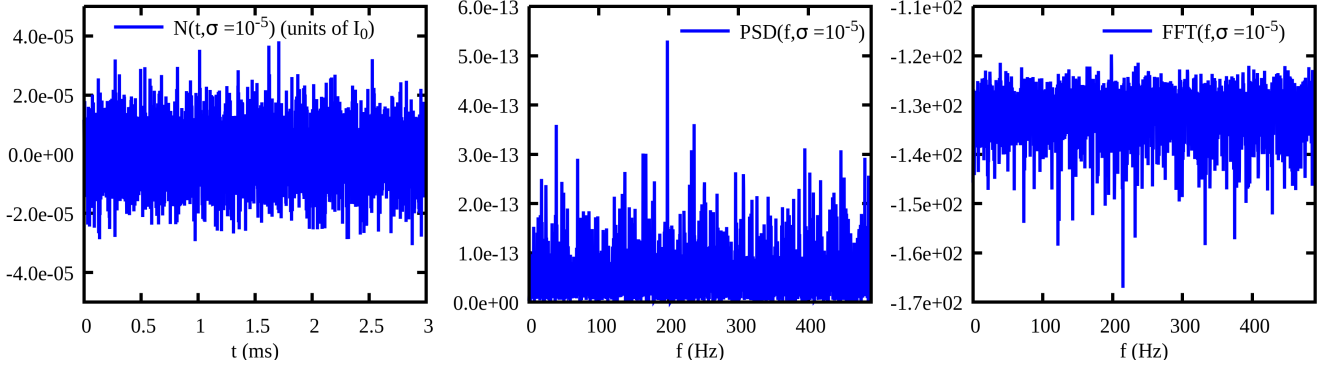


FIG. 5. The Gaussian noise signals $\mathbf{N}(t, \sigma^2 = 1.0 \times 10^{-5}, \xi = 0)$ in the time domain (left panels), its power spectral densities $\mathbf{PSD}(f, \sigma^2 = 1.0 \times 10^{-5}, \xi = 0)$ (middle panels) and its FFT result $\mathbf{FFT}(f, \sigma^2 = 1.0 \times 10^{-5}, \xi = 0)$ (right panels).

Similarly, we obtain the quantity $\Theta_{A+\mathbf{N}}(\tau)$ in the AWVA scheme with the noise $\mathbf{N}(t, \sigma^2)$, and the $\Theta_{A+\mathbf{N}}(\tau)$ is defined as

$$\begin{aligned} \Theta_{A+\mathbf{N}}(t; \tau) &= \int_t I_{21+\mathbf{N}}^{\text{out}}(t; \tau) \times I_{22+\mathbf{N}}^{\text{out}}(t) dt \\ &= \Theta_A(t; \tau) + \Theta_{21\mathbf{N}}(t; \tau) + \Theta_{22\mathbf{N}}(t; \tau) + \Theta_{\mathbf{N}\mathbf{N}}(t; \tau) \end{aligned} \quad (14)$$

with

$$\Theta_{21\mathbf{N}}(t; \tau) = \int_t I_{21}^{\text{out}}(t; \tau) \times \mathbf{N}(t, \sigma^2, \xi) dt, \quad (15)$$

$$\Theta_{22\mathbf{N}}(t; \tau) = \int_t I_{22}^{\text{out}}(t) \times \mathbf{N}(t, \sigma^2, \xi) dt. \quad (16)$$

However, due to the non-correlation between the signal and the random noise, we obtain that $\Theta_{21\mathbf{N}}(t; \tau) = \Theta_{22\mathbf{N}}(t; \tau) = 0$. Finally, we can get the relation $\Theta_{A+\mathbf{N}}(t; \tau) = \Theta_A(t; \tau)$ from the theoretical analysis when the integral time t is infinite, which means that the noise has no influence on evaluating the values of Θ .

Note that the "infinite" is a relative concept: when there are enough integral nodes (sample time) in the integral time t , the integral time can also be regarded as infinite. In conclusion, the equality $\Theta_{A+\mathbf{N}}(\tau) = \Theta_A(\tau)$ represents that the AWVA scheme has strong robustness¹ against noises. The features of the realistic noises are indeed more complicated than the features of the Gaussian noise [24–27]. However, it is necessary to first consider the effects of the strong Gaussian noise on the weak measurements theoretical, and the simulation results are shown in the next section.

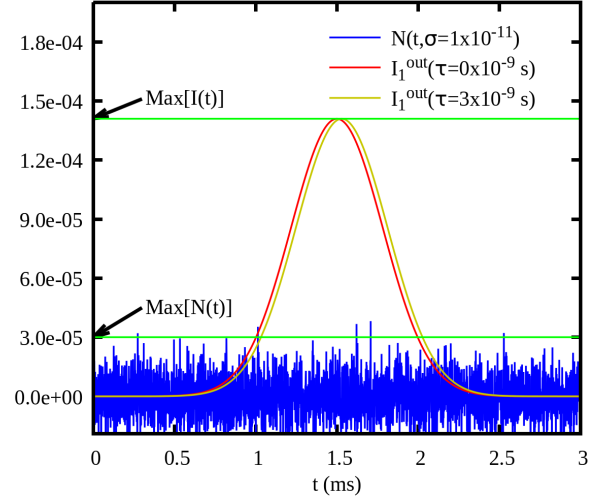


FIG. 6. An example of estimating the SNR in WVA scheme and AWVA scheme under the Gaussian white noise $\mathbf{N}(t, \sigma^2 = 10^{-11}, \xi = 0)$.

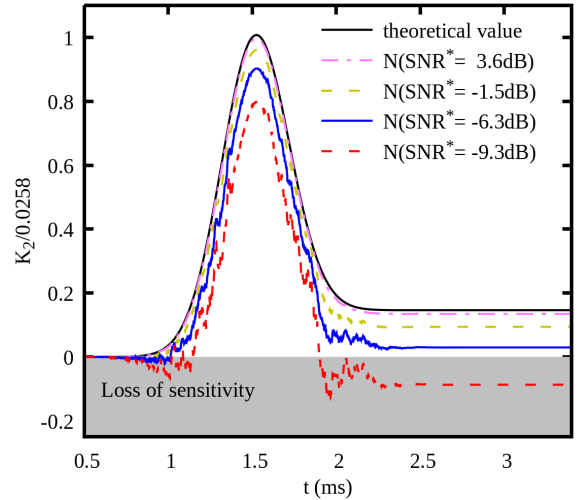


FIG. 7. The dependence of the sensitivity on the integral time t in the AWVA scheme. The gray band represents the measurements failing to effectively detect the final signal.

¹ The "robustness" of the control system refers to the ability of the system to keep certain performance invariable under the disturbance(noise) of uncertainty

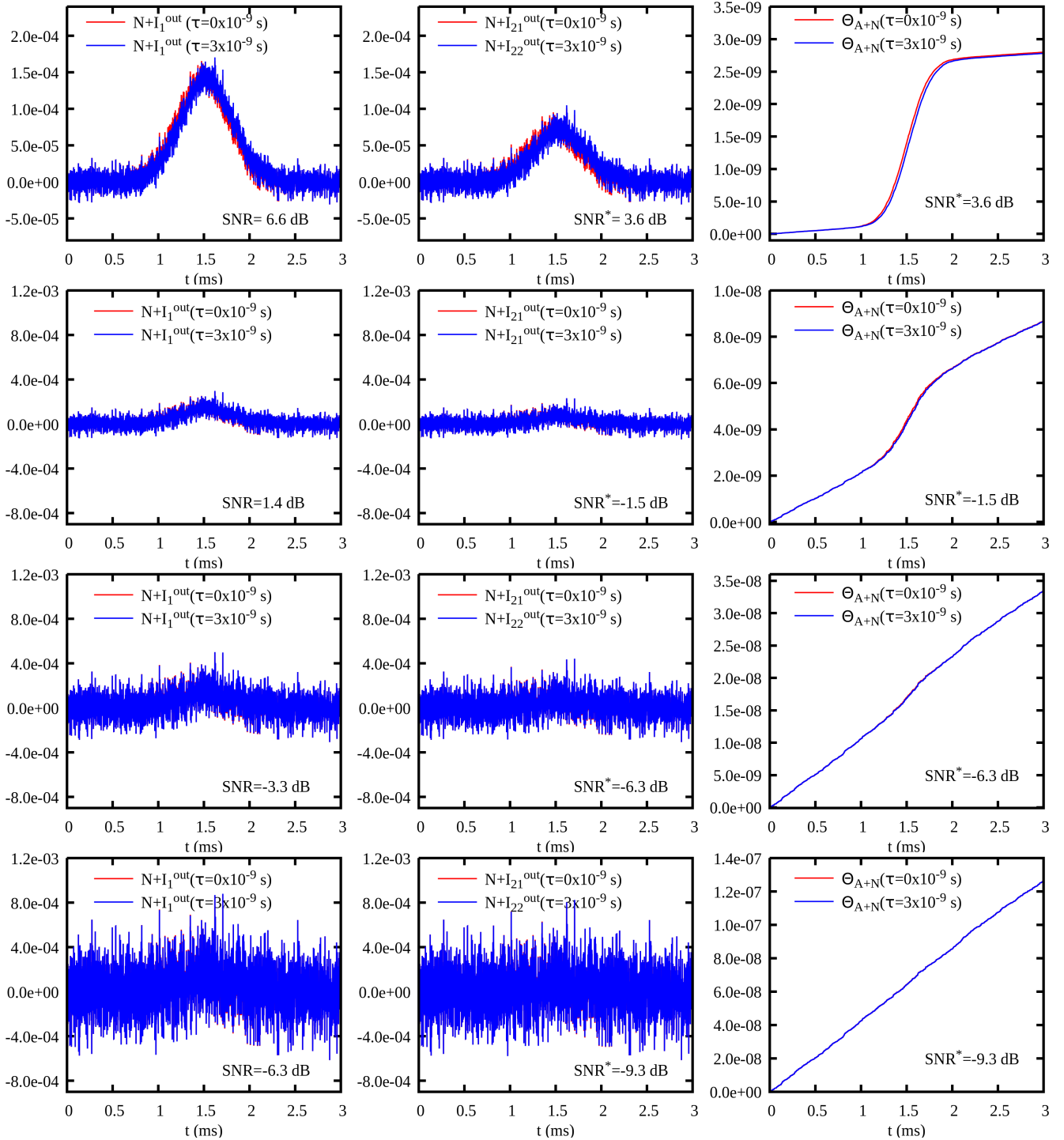


FIG. 8. The simulation results in two schemes under the Gaussian White noise $\mathbf{N}(t, \sigma^2, \xi = 000)$ with different SNR. Left panels: the signals $I_1^{out}(t; \tau)$ in the WVA scheme. Middle panels: the signals $I_{21}^{out}(t; \tau)$ and $I_{22}^{out}(t; \tau)$ in the AWVA scheme. Right panels: the signals Θ_{A+N} in the AWVA scheme. The units of the qualities $I_1^{out}(t; \tau)$, $I_{21}^{out}(t; \tau)$ and $I_{22}^{out}(t; \tau)$ are units of I_0 , the quality I_A^{AC} is units of voltage.

IV. NUMERICAL RESULTS

After adding the Gaussian white noise with different SNR to the signals, we fit the peak shift δt in the

WVA scheme and compute the values of Θ in the AWVA scheme respectively. In our simulation, the initial tem-

TABLE I. Parameters and some characteristic numerical results (dimensional quantities in unit of s) of measuring time shift $\tau = 3.0 \times 10^{-9}$ under Gaussian noise with different SNR in the WVA scheme. The contents E_{t_0} and E_{t_τ} in parentheses represent the standard error for estimating the time shifts δt_0 and δt_τ respectively. The data in red means the measurement is invalid. $\mathbf{N}(\xi = 000)$, $\mathbf{N}(\xi = 100)$... $\mathbf{N}(\xi = 600)$ represent the multiple measurements with the different initial time.

SNR	Noise	$\delta t_0 (\pm E_{t_0})$	$\delta t_\tau (\pm E_{t_\tau})$	$K_1 (\pm E_1)$
-	no-noise	$0.00 \times 10^{-3} (\pm 1.8 \times 10^{-12})$	$3.00 \times 10^{-5} (\pm 1.8 \times 10^{-12})$	$10.0 \times 10^3 (\pm 1.21 \times 10^{-3})$
6.6	$\mathbf{N}(\xi = 000)$	$9.20 \times 10^{-7} (\pm 1.21 \times 10^{-6})$	$3.07 \times 10^{-5} (\pm 1.21 \times 10^{-6})$	$9.92 \times 10^3 (\pm 0.81 \times 10^3)$
	$\mathbf{N}(\xi = 100)$	$1.25 \times 10^{-6} (\pm 1.24 \times 10^{-6})$	$3.11 \times 10^{-5} (\pm 1.24 \times 10^{-6})$	$9.95 \times 10^3 (\pm 0.82 \times 10^3)$
	$\mathbf{N}(\xi = 200)$	$2.33 \times 10^{-6} (\pm 1.20 \times 10^{-6})$	$3.23 \times 10^{-5} (\pm 1.20 \times 10^{-6})$	$9.99 \times 10^3 (\pm 0.80 \times 10^3)$
	$\mathbf{N}(\xi = 300)$	$-1.30 \times 10^{-7} (\pm 1.21 \times 10^{-6})$	$2.97 \times 10^{-5} (\pm 1.21 \times 10^{-6})$	$9.90 \times 10^3 (\pm 0.81 \times 10^3)$
	$\mathbf{N}(\xi = 400)$	$-2.90 \times 10^{-7} (\pm 1.18 \times 10^{-6})$	$2.98 \times 10^{-5} (\pm 1.18 \times 10^{-6})$	$9.93 \times 10^3 (\pm 0.78 \times 10^3)$
	$\mathbf{N}(\xi = 500)$	$2.99 \times 10^{-6} (\pm 1.20 \times 10^{-6})$	$3.32 \times 10^{-5} (\pm 1.20 \times 10^{-6})$	$10.0 \times 10^3 (\pm 0.80 \times 10^3)$
	$\mathbf{N}(\xi = 600)$	$-7.90 \times 10^{-7} (\pm 1.21 \times 10^{-6})$	$2.92 \times 10^{-5} (\pm 1.21 \times 10^{-6})$	$9.75 \times 10^3 (\pm 0.81 \times 10^3)$
1.4	$\mathbf{N}(\xi = 000)$	$3.83 \times 10^{-6} (\pm 5.28 \times 10^{-6})$	$3.29 \times 10^{-5} (\pm 5.29 \times 10^{-6})$	$9.69 \times 10^3 (\pm 3.52 \times 10^3)$
	$\mathbf{N}(\xi = 100)$	$5.62 \times 10^{-6} (\pm 5.49 \times 10^{-6})$	$3.51 \times 10^{-5} (\pm 5.47 \times 10^{-6})$	$9.82 \times 10^3 (\pm 3.65 \times 10^3)$
	$\mathbf{N}(\xi = 200)$	$1.05 \times 10^{-5} (\pm 5.40 \times 10^{-6})$	$4.05 \times 10^{-5} (\pm 5.36 \times 10^{-6})$	$10.0 \times 10^3 (\pm 3.59 \times 10^3)$
	$\mathbf{N}(\xi = 300)$	$-5.70 \times 10^{-7} (\pm 5.28 \times 10^{-6})$	$2.85 \times 10^{-5} (\pm 5.29 \times 10^{-6})$	$9.69 \times 10^3 (\pm 3.52 \times 10^3)$
	$\mathbf{N}(\xi = 400)$	$-1.33 \times 10^{-6} (\pm 5.32 \times 10^{-6})$	$2.89 \times 10^{-5} (\pm 5.32 \times 10^{-6})$	$10.0 \times 10^3 (\pm 3.55 \times 10^3)$
	$\mathbf{N}(\xi = 500)$	$1.36 \times 10^{-5} (\pm 5.53 \times 10^{-6})$	$4.45 \times 10^{-5} (\pm 5.48 \times 10^{-6})$	$10.3 \times 10^3 (\pm 3.66 \times 10^3)$
	$\mathbf{N}(\xi = 600)$	$-3.5 \times 10^{-6} (\pm 5.40 \times 10^{-6})$	$2.65 \times 10^{-5} (\pm 5.41 \times 10^{-6})$	$10.0 \times 10^3 (\pm 3.60 \times 10^3)$
-3.3	$\mathbf{N}(\xi = 000)$	$7.63 \times 10^{-6} (\pm 1.13 \times 10^{-5})$	$3.57 \times 10^{-5} (\pm 1.14 \times 10^{-5})$	$9.35 \times 10^3 (\pm 7.53 \times 10^3)$
	$\mathbf{N}(\xi = 100)$	$1.26 \times 10^{-5} (\pm 1.20 \times 10^{-5})$	$4.13 \times 10^{-5} (\pm 1.18 \times 10^{-5})$	$9.56 \times 10^3 (\pm 7.93 \times 10^3)$
	$\mathbf{N}(\xi = 200)$	$2.38 \times 10^{-5} (\pm 1.21 \times 10^{-5})$	$5.37 \times 10^{-5} (\pm 1.19 \times 10^{-5})$	$9.96 \times 10^3 (\pm 7.93 \times 10^3)$
	$\mathbf{N}(\xi = 300)$	$-1.23 \times 10^{-6} (\pm 1.14 \times 10^{-5})$	$2.69 \times 10^{-5} (\pm 1.14 \times 10^{-6})$	$9.37 \times 10^3 (\pm 7.60 \times 10^3)$
	$\mathbf{N}(\xi = 400)$	$-3.21 \times 10^{-6} (\pm 1.20 \times 10^{-5})$	$2.74 \times 10^{-5} (\pm 1.19 \times 10^{-5})$	$10.2 \times 10^3 (\pm 7.93 \times 10^3)$
	$\mathbf{N}(\xi = 500)$	$1.2577 \times 10^{-3} (\pm 7.91 \times 10^{-5})$	$1.2682 \times 10^{-3} (\pm 7.96 \times 10^{-5})$	$0.35 \times 10^3 (\pm 52.6 \times 10^3)$
	$\mathbf{N}(\xi = 600)$	$-7.9 \times 10^{-6} (\pm 1.20 \times 10^{-5})$	$2.22 \times 10^{-5} (\pm 1.21 \times 10^{-5})$	$10.0 \times 10^3 (\pm 8.00 \times 10^3)$
-6.6	$\mathbf{N}(\xi = 000)$	$1.23 \times 10^{-5} (\pm 2.12 \times 10^{-5})$	$3.87 \times 10^{-5} (\pm 2.14 \times 10^{-5})$	$8.80 \times 10^3 (\pm 14.2 \times 10^3)$
	$\mathbf{N}(\xi = 100)$	$2.52 \times 10^{-5} (\pm 2.28 \times 10^{-5})$	$5.22 \times 10^{-5} (\pm 2.23 \times 10^{-5})$	$9.82 \times 10^3 (\pm 15.1 \times 10^3)$
	$\mathbf{N}(\xi = 200)$	$7.61 \times 10^{-4} (\pm 3.93 \times 10^{-5})$	$7.64 \times 10^{-4} (\pm 3.98 \times 10^{-5})$	$0.12 \times 10^3 (\pm 26.4 \times 10^3)$
	$\mathbf{N}(\xi = 300)$	$-2.40 \times 10^{-6} (\pm 2.14 \times 10^{-5})$	$2.41 \times 10^{-5} (\pm 2.15 \times 10^{-5})$	$8.83 \times 10^3 (\pm 14.3 \times 10^3)$
	$\mathbf{N}(\xi = 400)$	$-6.60 \times 10^{-6} (\pm 2.42 \times 10^{-5})$	$2.41 \times 10^{-5} (\pm 2.42 \times 10^{-5})$	$10.2 \times 10^3 (\pm 16.1 \times 10^3)$
	$\mathbf{N}(\xi = 500)$	$1.4261 \times 10^{-3} (\pm 30.0 \times 10^{-5})$	$1.4259 \times 10^{-3} (\pm 29.2 \times 10^{-5})$	$-0.06 \times 10^3 (\pm 190 \times 10^3)$
	$\mathbf{N}(\xi = 600)$	$-1.0995 \times 10^{-3} (\pm 3.75 \times 10^{-5})$	$-1.0961 \times 10^{-3} (\pm 3.89 \times 10^{-5})$	$1.13 \times 10^3 (\pm 25.4 \times 10^3)$

poral probe was chosen as:

$$I_1^{in}(t; \tau) = |\langle q | \Psi_i \rangle|^2 = \frac{1}{(2\pi \times 0.0002^2)^{1/4}} e^{-\frac{(t-0.0015)^2}{0.0004^2}}. \quad (17)$$

where I_0 is set as unit, the angle for post-selection was set at $\alpha = 0.01$ rad. The measured results along with various noises are shown in Fig. 8. On this basis we compare the sensitivity and the stability (robustness) of the two schemes.

A. The signal-to-noise rate

Though the Fisher information [23, 32, 37, 38] is widely used to estimate the SNR in the standard weak measurement, it only represents the statistical error. Herein, we use a more general definition of SNR in the WVA scheme:

$$\text{SNR} = 10 \times \log \frac{\text{Max}[I_1^{\text{out}}(t)]}{\text{Max}[\mathbf{N}(t)]}, \quad (18)$$

where $\text{Max}[I(t)]$ and $\text{Max}[\mathbf{N}(t)]$ represent the maximum amplitude of the signal and the noise respectively. Take the example shown in Fig. 6, which gives $\text{SNR} = 10 \times \log \frac{1.4 \times 10^{-4}}{3.0 \times 10^{-5}} = 6.69$ dB. The numerical results in the WVA scheme with various noises are presented in Table. I.

TABLE II. Parameters and some characteristic numerical results of measuring time shift $\tau = 3.0 \times 10^{-9}$ under Gaussian noise with different SNR in the AWVA scheme. See the text for definition of SNR and SNR*. The quantity Θ_0 and Θ_τ are measured at $t = 1.5\text{ms}$. $\mathbf{N}(\xi = 000)$, $\mathbf{N}(\xi = 100)$... $\mathbf{N}(\xi = 600)$ represent the multiple measurements with the different initial times. The content $\pm E_2$ in parentheses represents the statistical error.

SNR	SNR*	Noise	Θ_0	Θ_τ	$\Delta\Theta$	K_2^M	$\bar{K}_2(\pm E_2)$
-	-	no-noise	1.2442×10^{-9}	1.1666×10^{-9}	7.76×10^{-11}	0.0258	
6.6	3.6	$\mathbf{N}(\xi = 000)$	1.3979×10^{-9}	1.3211×10^{-9}	7.68×10^{-11}	0.0256	$0.02585(\pm 4.5 \times 10^{-5})$
		$\mathbf{N}(\xi = 100)$	1.4028×10^{-9}	1.3255×10^{-9}	7.73×10^{-11}	0.0257	
		$\mathbf{N}(\xi = 200)$	1.3603×10^{-9}	1.2841×10^{-9}	7.62×10^{-11}	0.0254	
		$\mathbf{N}(\xi = 300)$	1.4412×10^{-9}	1.3623×10^{-9}	7.89×10^{-11}	0.0263	
		$\mathbf{N}(\xi = 400)$	1.4050×10^{-9}	1.3264×10^{-9}	7.86×10^{-11}	0.0262	
		$\mathbf{N}(\xi = 500)$	1.3552×10^{-9}	1.2784×10^{-9}	7.68×10^{-11}	0.0256	
		$\mathbf{N}(\xi = 600)$	1.4176×10^{-9}	1.3393×10^{-9}	7.83×10^{-11}	0.0261	
1.4	-1.5	$\mathbf{N}(\xi = 000)$	4.3769×10^{-9}	4.3033×10^{-9}	7.36×10^{-11}	0.0245	$0.02570(\pm 2.1 \times 10^{-4})$
		$\mathbf{N}(\xi = 100)$	4.4760×10^{-9}	4.4000×10^{-9}	7.60×10^{-11}	0.0253	
		$\mathbf{N}(\xi = 200)$	4.1145×10^{-9}	4.0431×10^{-9}	7.14×10^{-11}	0.0238	
		$\mathbf{N}(\xi = 300)$	4.6210×10^{-9}	4.5375×10^{-9}	8.35×10^{-11}	0.0278	
		$\mathbf{N}(\xi = 400)$	4.1843×10^{-9}	4.1025×10^{-9}	8.18×10^{-11}	0.0272	
		$\mathbf{N}(\xi = 500)$	4.0047×10^{-9}	3.9307×10^{-9}	7.40×10^{-11}	0.0246	
		$\mathbf{N}(\xi = 600)$	4.4371×10^{-9}	4.3568×10^{-9}	8.03×10^{-11}	0.0267	
-3.3	-6.3	$\mathbf{N}(\xi = 000)$	1.69557×10^{-8}	1.68871×10^{-8}	6.86×10^{-11}	0.0228	$0.02551(\pm 4.4 \times 10^{-4})$
		$\mathbf{N}(\xi = 100)$	1.74519×10^{-8}	1.73781×10^{-8}	7.38×10^{-11}	0.0246	
		$\mathbf{N}(\xi = 200)$	1.60328×10^{-8}	1.59693×10^{-8}	6.35×10^{-11}	0.0211	
		$\mathbf{N}(\xi = 300)$	1.76797×10^{-8}	1.75891×10^{-8}	9.06×10^{-11}	0.0302	
		$\mathbf{N}(\xi = 400)$	1.57258×10^{-8}	1.56390×10^{-8}	8.68×10^{-11}	0.0289	
		$\mathbf{N}(\xi = 500)$	1.54774×10^{-8}	1.54079×10^{-8}	6.95×10^{-11}	0.0231	
		$\mathbf{N}(\xi = 600)$	1.69902×10^{-8}	1.69064×10^{-8}	8.38×10^{-11}	0.0279	
-6.3	-9.3	$\mathbf{N}(\xi = 000)$	6.41677×10^{-8}	6.41081×10^{-8}	5.96×10^{-11}	0.0198	$0.02517(\pm 8.7 \times 10^{-4})$
		$\mathbf{N}(\xi = 100)$	6.61542×10^{-8}	6.60842×10^{-8}	7.00×10^{-11}	0.0233	
		$\mathbf{N}(\xi = 200)$	6.11064×10^{-8}	6.10569×10^{-8}	4.95×10^{-11}	0.0165	
		$\mathbf{N}(\xi = 300)$	6.62609×10^{-8}	6.61575×10^{-8}	10.3×10^{-11}	0.0344	
		$\mathbf{N}(\xi = 400)$	5.88171×10^{-8}	5.87212×10^{-8}	9.59×10^{-11}	0.0319	
		$\mathbf{N}(\xi = 500)$	5.88743×10^{-8}	5.88130×10^{-8}	6.13×10^{-11}	0.0204	
		$\mathbf{N}(\xi = 600)$	6.38743×10^{-8}	6.37845×10^{-8}	8.98×10^{-11}	0.0299	

For the measurements with the AWVA technique, we define the sensitivity SNR* as an intermediate step in the AWVA scheme and the sensitivity SNR* is obtained by

$$\text{SNR}^* = 10 \times \log \frac{\text{Max}[\mathbf{I}_{21}^{\text{out}}(t)]}{\text{Max}[\mathbf{N}(t)]}, \quad (19)$$

In the WVA scheme, the position of noises in the optical path has no effect on the calculation of SNR in our simulation, because there is only a single optical path in the WVA scheme. However, in the AWVA scheme, it is worth noting that the 50:50 beam splitter (shown in Fig. 2) will reduce the strength of the signal. Thus, where the noises appear will lead to the different values of SNR*. When the noise is assumed to occur only in the optical path before the BS element, the value of SNR* is

equal to the value of SNR. When the noise is assumed to occur only in the optical path after the BS element, the value of SNR* is reduced and $\text{SNR}^* = 0.5\text{SNR}$. In addition, the value of SNR* will calculate at the range of $0.5\text{SNR} < \text{SNR}^* < \text{SNR}$ when the noises occur throughout the optical path in the AWVA scheme. In this paper, in order to highlight the advantages of the scheme, we investigate the lowest $\text{SNR}^* = 0.5\text{SNR}$, because the lower the SNR*, the harder it is to detect a useful signal.

Note that the relationship $\Theta_{A+N}(\tau) = \Theta_A(\tau)$ is only true if the integral time is infinite in Eq. (14). On the other hand, the sampling time (corresponding to the integral time) is finite and the pseudo-random number generator can not generate truly random numbers. Thus, the various noises will affect the value of Θ and cause un-

TABLE III. The numerical results (dimensional quantities in unit of s) for measuring the different τ under the strong noise at SNR= -6.3 dB in the WVA scheme. The contents E_{t_0} and E_{t_τ} in parentheses represent the standard error for estimating the time shifts δt_0 and δt_τ respectively. The data in red means the measurement is invalid. $\mathbf{N}(\xi = 000)$, $\mathbf{N}(\xi = 100)$... $\mathbf{N}(\xi = 600)$ represent the multiple measurements with the different initial times.

τ	Noise	$\delta t_0 (\pm E_{t_0})$	$\delta t_\tau (\pm E_{t_\tau})$	$K_1 (\pm E_1)$
6×10^{-9}	$\mathbf{N}(\xi = 000)$	$1.23 \times 10^{-5} (\pm 2.12 \times 10^{-5})$	$6.57 \times 10^{-5} (\pm 2.16 \times 10^{-5})$	$8.90 \times 10^3 (\pm 7.13 \times 10^3)$
	$\mathbf{N}(\xi = 100)$	$2.52 \times 10^{-5} (\pm 2.28 \times 10^{-5})$	$7.85 \times 10^{-5} (\pm 2.20 \times 10^{-5})$	$8.88 \times 10^3 (\pm 7.46 \times 10^3)$
	$\mathbf{N}(\xi = 200)$	$7.6086 \times 10^{-4} (\pm 3.93 \times 10^{-5})$	$7.7576 \times 10^{-4} (\pm 4.28 \times 10^{-5})$	$2.48 \times 10^3 (\pm 13.6 \times 10^3)$
	$\mathbf{N}(\xi = 300)$	$-2.40 \times 10^{-6} (\pm 2.14 \times 10^{-5})$	$5.07 \times 10^{-5} (\pm 2.15 \times 10^{-5})$	$8.85 \times 10^3 (\pm 7.15 \times 10^3)$
	$\mathbf{N}(\xi = 400)$	$-6.60 \times 10^{-6} (\pm 2.42 \times 10^{-5})$	$5.49 \times 10^{-5} (\pm 2.41 \times 10^{-5})$	$10.2 \times 10^3 (\pm 8.05 \times 10^3)$
	$\mathbf{N}(\xi = 500)$	$1.4261 \times 10^{-3} (\pm 30.0 \times 10^{-5})$	$1.4251 \times 10^{-3} (\pm 28.2 \times 10^{-5})$	$-0.16 \times 10^3 (\pm 98.6 \times 10^3)$
	$\mathbf{N}(\xi = 600)$	$-1.0995 \times 10^{-3} (\pm 3.75 \times 10^{-5})$	$-1.0920 \times 10^{-3} (\pm 4.07 \times 10^{-5})$	$1.25 \times 10^3 (\pm 13.0 \times 10^3)$
9×10^{-9}	$\mathbf{N}(\xi = 000)$	$1.23 \times 10^{-5} (\pm 2.12 \times 10^{-5})$	$9.34 \times 10^{-5} (\pm 2.19 \times 10^{-5})$	$9.01 \times 10^3 (\pm 4.84 \times 10^3)$
	$\mathbf{N}(\xi = 100)$	$2.52 \times 10^{-5} (\pm 2.28 \times 10^{-5})$	$10.4 \times 10^{-5} (\pm 2.18 \times 10^{-5})$	$8.75 \times 10^3 (\pm 5.22 \times 10^3)$
	$\mathbf{N}(\xi = 200)$	$7.6086 \times 10^{-4} (\pm 3.93 \times 10^{-5})$	$7.8843 \times 10^{-4} (\pm 4.58 \times 10^{-5})$	$3.05 \times 10^3 (\pm 9.45 \times 10^3)$
	$\mathbf{N}(\xi = 300)$	$-2.40 \times 10^{-6} (\pm 2.14 \times 10^{-5})$	$7.72 \times 10^{-5} (\pm 2.16 \times 10^{-5})$	$8.84 \times 10^3 (\pm 4.77 \times 10^3)$
	$\mathbf{N}(\xi = 400)$	$-6.60 \times 10^{-6} (\pm 2.42 \times 10^{-5})$	$8.58 \times 10^{-5} (\pm 2.39 \times 10^{-5})$	$10.3 \times 10^3 (\pm 5.34 \times 10^3)$
	$\mathbf{N}(\xi = 500)$	$1.4261 \times 10^{-3} (\pm 30.0 \times 10^{-5})$	$1.4238 \times 10^{-3} (\pm 26.8 \times 10^{-5})$	$-0.25 \times 10^3 (\pm 65.5 \times 10^3)$
	$\mathbf{N}(\xi = 600)$	$-1.0995 \times 10^{-3} (\pm 3.75 \times 10^{-5})$	$-1.0869 \times 10^{-3} (\pm 4.31 \times 10^{-5})$	$1.38 \times 10^3 (\pm 8.95 \times 10^3)$
12×10^{-9}	$\mathbf{N}(\xi = 000)$	$1.23 \times 10^{-5} (\pm 2.12 \times 10^{-5})$	$12.2 \times 10^{-5} (\pm 2.23 \times 10^{-5})$	$9.12 \times 10^3 (\pm 3.62 \times 10^3)$
	$\mathbf{N}(\xi = 100)$	$2.52 \times 10^{-5} (\pm 2.28 \times 10^{-5})$	$13.1 \times 10^{-5} (\pm 2.18 \times 10^{-5})$	$8.77 \times 10^3 (\pm 3.75 \times 10^3)$
	$\mathbf{N}(\xi = 200)$	$7.6086 \times 10^{-4} (\pm 3.93 \times 10^{-5})$	$8.1703 \times 10^{-4} (\pm 5.26 \times 10^{-5})$	$4.68 \times 10^3 (\pm 7.65 \times 10^3)$
	$\mathbf{N}(\xi = 300)$	$-2.40 \times 10^{-6} (\pm 2.14 \times 10^{-5})$	$10.4 \times 10^{-5} (\pm 2.16 \times 10^{-5})$	$9.21 \times 10^3 (\pm 2.68 \times 10^3)$
	$\mathbf{N}(\xi = 400)$	$-6.60 \times 10^{-6} (\pm 2.42 \times 10^{-5})$	$11.7 \times 10^{-5} (\pm 2.37 \times 10^{-5})$	$10.3 \times 10^3 (\pm 3.99 \times 10^3)$
	$\mathbf{N}(\xi = 500)$	$1.4261 \times 10^{-3} (\pm 30.0 \times 10^{-5})$	$1.4217 \times 10^{-3} (\pm 25.2 \times 10^{-5})$	$-0.36 \times 10^3 (\pm 45.8 \times 10^3)$
	$\mathbf{N}(\xi = 600)$	$-1.0995 \times 10^{-3} (\pm 4.66 \times 10^{-5})$	$-1.0797 \times 10^{-3} (\pm 4.63 \times 10^{-5})$	$1.65 \times 10^3 (\pm 7.40 \times 10^3)$
15×10^{-9}	$\mathbf{N}(\xi = 000)$	$1.23 \times 10^{-5} (\pm 2.12 \times 10^{-5})$	$15.7 \times 10^{-5} (\pm 2.27 \times 10^{-5})$	$9.23 \times 10^3 (\pm 2.92 \times 10^3)$
	$\mathbf{N}(\xi = 100)$	$2.52 \times 10^{-5} (\pm 2.28 \times 10^{-5})$	$15.6 \times 10^{-5} (\pm 2.18 \times 10^{-5})$	$8.76 \times 10^3 (\pm 2.96 \times 10^3)$
	$\mathbf{N}(\xi = 200)$	$7.6086 \times 10^{-4} (\pm 3.93 \times 10^{-5})$	$8.6756 \times 10^{-4} (\pm 6.45 \times 10^{-5})$	$7.11 \times 10^3 (\pm 6.92 \times 10^3)$
	$\mathbf{N}(\xi = 300)$	$-2.40 \times 10^{-6} (\pm 2.14 \times 10^{-5})$	$13.1 \times 10^{-5} (\pm 2.16 \times 10^{-5})$	$8.86 \times 10^3 (\pm 2.86 \times 10^3)$
	$\mathbf{N}(\xi = 400)$	$-6.60 \times 10^{-6} (\pm 2.42 \times 10^{-5})$	$14.7 \times 10^{-5} (\pm 2.34 \times 10^{-5})$	$10.3 \times 10^3 (\pm 3.17 \times 10^3)$
	$\mathbf{N}(\xi = 500)$	$1.4261 \times 10^{-3} (\pm 30.0 \times 10^{-5})$	$1.4187 \times 10^{-3} (\pm 24.0 \times 10^{-5})$	$-0.49 \times 10^3 (\pm 36.0 \times 10^3)$
	$\mathbf{N}(\xi = 600)$	$-1.0995 \times 10^{-3} (\pm 3.75 \times 10^{-5})$	$-1.0687 \times 10^{-3} (\pm 5.24 \times 10^{-5})$	$2.05 \times 10^3 (\pm 5.99 \times 10^3)$

certainty in estimating the sensitivity of the scheme with the AWVA technique. In addition, the analysis of the sensitivity to various noises and the discussion of comparison with these results in the WVA scheme are shown in the next subsection.

B. The sensitivity with the standard error

In order to calculate the sensitivity in the two schemes, we did the simulation with both schemes with the time shift τ . In the WVA scheme, the sensitivity is defined as

$$K_1 = \frac{\Delta(\delta t)}{\Delta(\tau)} = \frac{\delta t_\tau - \delta t_0}{\tau}, \quad (20)$$

where peak value shift δt_0 of the temporal pointer and its standard error E_{t_0} represent the results with the time shift $\tau = 0$ s. The peak value shift δt_τ of the temporal pointer and its standard error E_{t_τ} are obtained by fitting the Gaussian profile of the signal $I_1^{out}(t, \tau)$ with least square method. Then, the statistical error E_1 for estimating the value of K_1 can be calculated from Eq. (20) with the law of error propagation: $E_1 = (|E_{t_\tau}| + |E_{t_0}|)/\tau$. Finally, the sensitivity K_1 with its the statistical error E_1 under different simulation conditions are shown in Table I and Table III.

Note that the quantities measured in the AWVA scheme are the values of Θ , therefore, the sensitivity in the AWVA scheme is defined as:

$$K_2(t) = \frac{\Delta[\Theta(t; \tau)]}{\Delta(\tau)} = \frac{\Theta_0 - \Theta_\tau}{\tau}, \quad (21)$$

TABLE IV. Parameters and some characteristic numerical results for measuring the different τ under the strong noise at SNR=-6.3 dB in the AWVA scheme. The quantity Θ_0 and Θ_τ are measured at $t = 1.5$ ms. $\mathbf{N}(\xi = 000)$, $\mathbf{N}(\xi = 100)$... $\mathbf{N}(\xi = 600)$ represent the multiple measurements with the different initial times. The content $\pm E_2$ in parentheses represents the statistical error.

τ	Noise	Θ_0	Θ_τ	$\Delta\Theta$	K_2^M	$\bar{K}_2 (\pm E_2)$
6×10^{-9}	$\mathbf{N}(\xi = 000)$	6.41677×10^{-8}	6.40403×10^{-8}	12.7×10^{-11}	0.0212	$0.02608(\pm 9.5 \times 10^{-4})$
	$\mathbf{N}(\xi = 100)$	6.61542×10^{-8}	6.60088×10^{-8}	14.5×10^{-11}	0.0242	
	$\mathbf{N}(\xi = 200)$	6.11064×10^{-8}	6.10021×10^{-8}	10.4×10^{-11}	0.0174	
	$\mathbf{N}(\xi = 300)$	6.62609×10^{-8}	6.60479×10^{-8}	21.3×10^{-11}	0.0355	
	$\mathbf{N}(\xi = 400)$	5.88171×10^{-8}	5.86211×10^{-8}	19.6×10^{-11}	0.0326	
	$\mathbf{N}(\xi = 500)$	5.88743×10^{-8}	5.87495×10^{-8}	12.4×10^{-11}	0.0208	
	$\mathbf{N}(\xi = 600)$	6.38743×10^{-8}	6.36885×10^{-8}	18.5×10^{-11}	0.0309	
9×10^{-9}	$\mathbf{N}(\xi = 000)$	6.41677×10^{-8}	6.39661×10^{-8}	20.2×10^{-11}	0.0224	$0.02677(\pm 9.4 \times 10^{-4})$
	$\mathbf{N}(\xi = 100)$	6.61542×10^{-8}	6.59294×10^{-8}	22.5×10^{-11}	0.0249	
	$\mathbf{N}(\xi = 200)$	6.11064×10^{-8}	6.09433×10^{-8}	18.1×10^{-11}	0.0181	
	$\mathbf{N}(\xi = 300)$	6.62609×10^{-8}	6.59344×10^{-8}	32.6×10^{-11}	0.0362	
	$\mathbf{N}(\xi = 400)$	5.88171×10^{-8}	5.85185×10^{-8}	29.8×10^{-11}	0.0331	
	$\mathbf{N}(\xi = 500)$	5.88743×10^{-8}	5.86848×10^{-8}	18.9×10^{-11}	0.0210	
	$\mathbf{N}(\xi = 600)$	6.38743×10^{-8}	6.35884×10^{-8}	28.6×10^{-11}	0.0317	
12×10^{-9}	$\mathbf{N}(\xi = 000)$	6.41677×10^{-8}	6.38875×10^{-8}	28.1×10^{-11}	0.0233	$0.02731(\pm 9.5 \times 10^{-4})$
	$\mathbf{N}(\xi = 100)$	6.61542×10^{-8}	6.58475×10^{-8}	30.6×10^{-11}	0.0255	
	$\mathbf{N}(\xi = 200)$	6.11064×10^{-8}	6.08820×10^{-8}	22.4×10^{-11}	0.0187	
	$\mathbf{N}(\xi = 300)$	6.62609×10^{-8}	6.58193×10^{-8}	44.1×10^{-11}	0.0368	
	$\mathbf{N}(\xi = 400)$	5.88171×10^{-8}	5.84153×10^{-8}	40.1×10^{-11}	0.0335	
	$\mathbf{N}(\xi = 500)$	5.88743×10^{-8}	5.86200×10^{-8}	25.4×10^{-11}	0.0211	
	$\mathbf{N}(\xi = 600)$	6.38743×10^{-8}	6.34863×10^{-8}	38.8×10^{-11}	0.0323	
15×10^{-9}	$\mathbf{N}(\xi = 000)$	6.41677×10^{-8}	6.38063×10^{-8}	36.1×10^{-11}	0.0240	$0.02761(\pm 9.4 \times 10^{-4})$
	$\mathbf{N}(\xi = 100)$	6.61542×10^{-8}	6.57647×10^{-8}	38.9×10^{-11}	0.0259	
	$\mathbf{N}(\xi = 200)$	6.11064×10^{-8}	6.08196×10^{-8}	28.6×10^{-11}	0.0191	
	$\mathbf{N}(\xi = 300)$	6.62609×10^{-8}	6.57047×10^{-8}	55.6×10^{-11}	0.0370	
	$\mathbf{N}(\xi = 400)$	5.88171×10^{-8}	5.83133×10^{-8}	50.4×10^{-11}	0.0335	
	$\mathbf{N}(\xi = 500)$	5.88743×10^{-8}	5.85562×10^{-8}	31.8×10^{-11}	0.0212	
	$\mathbf{N}(\xi = 600)$	6.38743×10^{-8}	6.33844×10^{-8}	48.9×10^{-11}	0.0326	

where Θ_τ represents the result $\Theta_{A+N}(t; \tau)$ calculated from Eq. (15), Θ_0 represents the initial value of the measurement without the time shift τ and can be calculated from the dates I_{22+N}^{out} on APD2 in Fig. 2:

$$\Theta_0 = \int_t I_{22+N}^{out}(t) \times I_{22+N}^{out}(t) dt \quad (22)$$

Note that the sensitivity $K_2(t)$ depends on the scope of time integral t . The dependence of the sensitivity on t with various noises is shown in Fig. 7, and one can find that the maximum sensitivity K_2^M is achieved when integrate to $t = 1.5$ ms. In addition, we neglect the standard error of K_2^M , since K_2^M can be estimated by using a high vertical resolution oscilloscope. We show the maximum sensitivity K_2^M without standard errors in Table. II and Table. IV. In this paper, we define the central value \bar{K}_2

with its statistical error E_2 in the AWVA scheme, which is created by calculating the seven statistical averages of K_2^M with different measurements:

$$\bar{K}_2 = \sum_{i=1}^n K_2^M(i)/n, \quad E_2 = \text{Max}\{|\bar{K}_2 - K_2^M(i)|\}, \quad (23)$$

where the $K_2^M(i)$ represents the result of the i th measurement with the different value of ξ , n represents the total number of measurements and $n=7$. For different simulation conditions, the central value \bar{K}_2 with its statistical error E_2 in the AWVA scheme are displayed in Table II and Table IV. To compare the sensitivity in the two schemes, we further normalized them with their corresponding theoretical results in Fig. 9 and Fig. 10. Note that when the value of the sensitivity $K < 0$, corresponding to the "Loss of sensitivity" area, the measurement is

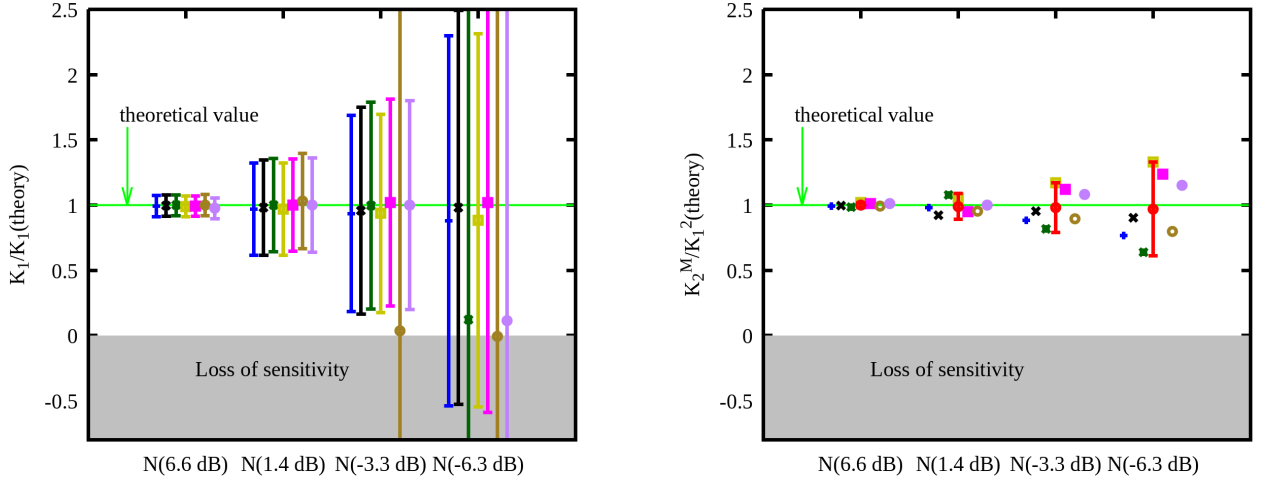


FIG. 9. The normalized sensitivity in the WVA scheme(left figure) and in the AWVA scheme(right figure) under the Gaussian noises with different SNR. The gray band represents the measurements failing to effectively detect the final signal. The "blue" dates represent Random seed " $\xi=000$ "; The "black" dates represent Random seed " $\xi=100$ "; The "dark-green" dates represent Random seed " $\xi=200$ "; The "dark-yellow" dates represent Random seed " $\xi=300$ "; The "magenta" dates represent Random seed " $\xi=400$ "; The "olive" dates represent Random seed " $\xi=500$ "; The "purple" dates represent Random seed " $\xi=600$ ". The "red" dates with the error bar represent the final results of seven statistical averages in the AWVA scheme.

invalid. The central value \bar{K}_2 with its statistical error E_2 in the AWVA scheme are displayed as the "red" dates with error bar in Fig. 9 and Fig. 10.

C. Effects of Gaussian white noise with different SNR

Fig. 8 displays the results in the two schemes under the Gaussian white noise $\mathbf{N}(\sigma = 10^{-5}, \xi = 000)$ with different SNRs. In addition, the corresponding results of the sensitivity are shown in Table. I. Combining the results of the normalized sensitivity in Fig. 9, we come to the following summaries of the effects of noises in the two schemes:

1). In general, the AWVA scheme outperforms the WVA scheme, because the statistical error of the normalized sensitivity in the AWVA scheme is much smaller than that in the WVA scheme at the same level of SNR. Note that our results may be obtained by assuming that the time resolution and the vertical resolution of the oscilloscope can meet the requirements of our scheme, where the vertical resolution of the oscilloscope limits the accuracy of the value of Θ . On the other hand, the signal processing modules(Fig. 3) do not need to be implemented in hardware if the weak measurement does not meet the real-time measurement and this progress may generate other noises. Thus, the results of Θ can be calculated mathematically after the measurement from the collected data on APD1 and APD2 of the scheme in Fig. 2.

2). There is no doubt that the intensity of noise significantly affects the results in both two schemes. As shown in Fig. 9, the statistical error of K_1 and \bar{K}_2 in-

crease, when the SNR is smaller. However, when the SNR is smaller than -3.3dB , the central values of the measurement under noises $\mathbf{N}(\text{SNR} = -3.3\text{dB}, \xi = 500)$, $\mathbf{N}(\text{SNR} = -6.3\text{dB}, \xi = 300)$, $\mathbf{N}(\text{SNR} = -6.3\text{dB}, \xi = 500)$ and $\mathbf{N}(\text{SNR} = -6.3\text{dB}, \xi = 600)$ deviates greatly from the theoretical value in WVA scheme. In addition, the measurements under noise at $\text{SNR} = -6.3\text{dB}$ in the WVA scheme are invalid due to the error bars extending into the "Loss of sensitivity" area. Meanwhile, under the strong noise with negative SNR, the scheme with the AWVA technique gives more accurate results with smaller statistical errors than the scheme with the WVA technique.

In conclusion, the advantage of the scheme with the VWVA technique is more obvious when the SNR is lower. Note that the statistical errors in the VWVA scheme get bigger when SNR is lower. Therefore, there is also a lower limit (corresponding to the minimum SNR) to how effective the VWVA scheme can be measured.

D. Effects of the coupling strength

In the two schemes for measuring the time shifts τ induced by a birefringent crystal, the time shift τ serves as the coupling strength in the weak measurements. Next, we will show the results with the two schemes at different coupling strengths τ . Note that this discussion is necessary due to the two schemes can be transformed to measure other physical quantities. In Fig. 10, we show the results of δt in the WVA scheme and the shift of $\Theta(t=1.5\text{ms})$ in the AWVA scheme, as well as their corresponding sensitivities, under the noise $\mathbf{N}(t, \sigma^2 = 4.0 \times 10^{-7})$ with

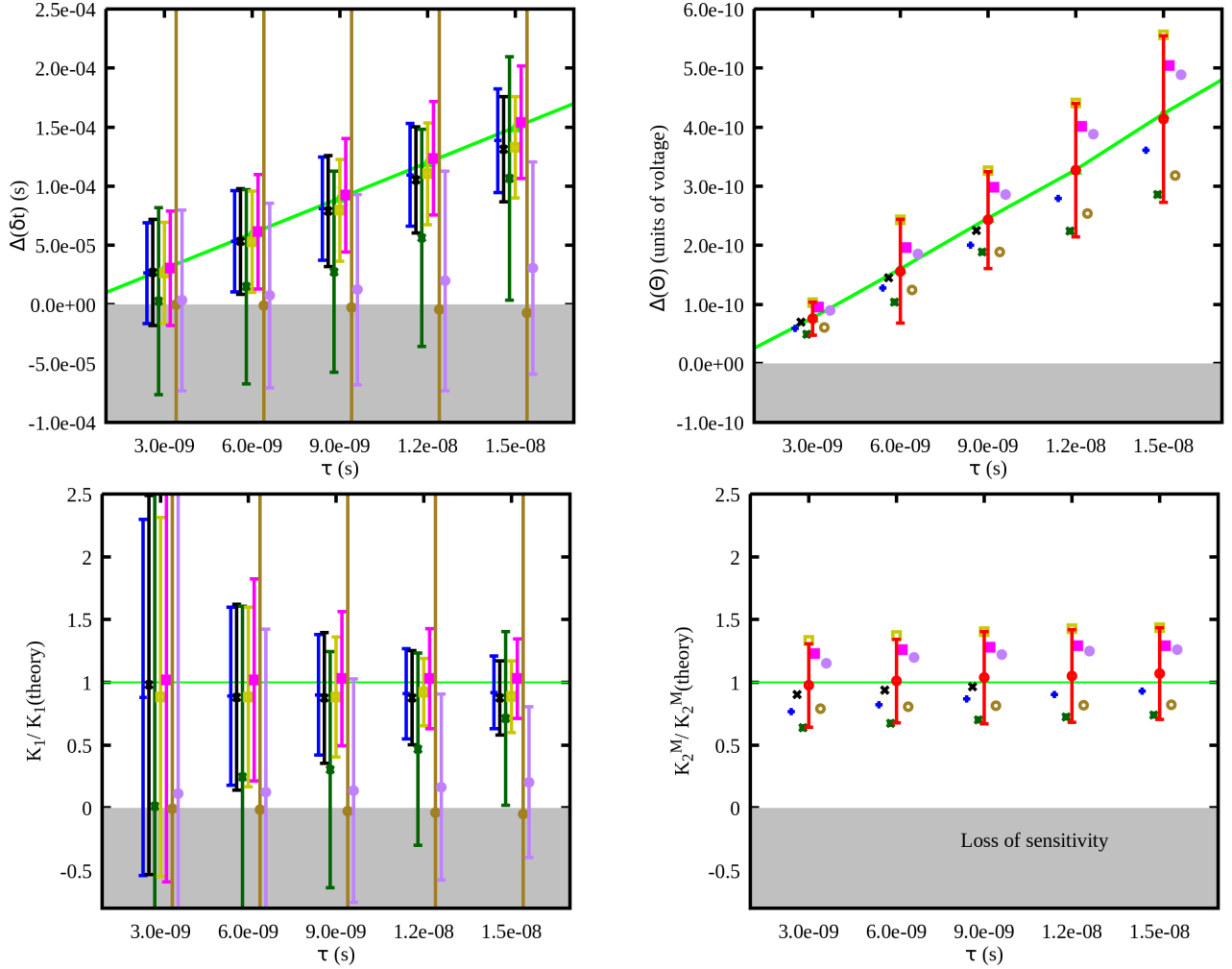


FIG. 10. The shifts $\Delta(\delta t)$ as well as the shifts $\Delta(\Theta)$ (upper panels), and the corresponding sensitivity (lower panels) with respect to the coupling strength τ under the noise $\mathbf{N}(t, \sigma^2 = 4.0 \times 10^{-7})$ with SNR = -6.3 dB. The left panel shows the results in the WVA scheme, and the right panel shows the results in the AWVA scheme. The results of the green line represent theoretical results in absence of noise while the other dates represent the simulation results under the noise $\mathbf{N}(t, \sigma^2 = 4.0 \times 10^{-7}, \xi)$. The gray band represents the measurements failing to effectively detect the final signal. The "blue" dates represent Random seed " $\xi=100$ "; The "dark-green" dates represent Random seed " $\xi=200$ "; The "dark-yellow" dates represent Random seed " $\xi=300$ "; The "magenta" dates represent Random seed " $\xi=400$ "; The "olive" dates represent Random seed " $\xi=500$ "; The "purple" dates represent Random seed " $\xi=600$ ". The "red" dates with the error bar represent the final results of seven statistical averages in the AWVA scheme.

SNR=-6.3 dB. Note that the sensitivity K_1 and \bar{K}_2 have been normalized to describe the deviation from the theoretical values. Fig. 10 shows the deviations of the results in the two schemes from the theoretical value. We come to the following summaries of the effects of the coupling strength in the two schemes:

(1). The upper panels in Fig. 10 display the shifts $\Delta(\delta t)$ in the WVA scheme and the shifts $\Delta(\Theta)$ in the AWVA scheme dependence of the coupling strength τ . Under the same noise with SNR = -6.3dB, the measurements with their error bars in the WVA scheme extending into the "Loss of sensitivity" area are invalid, while all the measurements in the AWVA scheme give valid results with statistical errors. Besides, the central values of mea-

asuring $\Delta(\Theta)$ in the AWVA scheme agree with the theoretical results in absence of noises. Nevertheless, the central values of measuring $\Delta(\delta t)$ in the WVA scheme deviated greatly from the theoretical values. In addition, the magnitudes of the statistical errors in the WVA scheme are independent of the coupling strength τ , and it is clear to verify that when discarding the measurements with the noise $\mathbf{N}(\sigma = 10^{-5}, \xi = 500)$ and $\mathbf{N}(\sigma = 10^{-5}, \xi = 600)$. While the magnitudes of the error bars in the AWVA scheme get bigger when the coupling strength τ increases.

(2). The lower panels in Fig. 10 display the normalized sensitivity K_1 and \bar{K}_2 dependence of the coupling strength τ . The results in the WVA scheme indicate that the statistical errors of estimating K_1 get smaller when

TABLE V. The numerical average results (dimensional quantities in unit of s) of multiple measurement time shift $\tau = 3.0 \times 10^{-9}$ s under Gaussian noise with different SNR.

SNR	$\delta\bar{t}_0(\pm\bar{E}_{t0})$	$\delta\bar{t}_\tau(\pm\bar{E}_{t\tau})$	$\Delta(\delta\bar{t})$	$\bar{K}_1(\pm\bar{E}_1)/1.0 \times 10^3$
6.6	$8.97 \times 10^{-7} (\pm 2.09 \times 10^{-6})$	$3.09 \times 10^{-5} (\pm 2.30 \times 10^{-6})$	$3.00 \times 10^{-5} (\pm 4.39 \times 10^{-6})$	1.000(± 0.146)
1.4	$4.02 \times 10^{-6} (\pm 9.58 \times 10^{-6})$	$3.38 \times 10^{-5} (\pm 1.07 \times 10^{-5})$	$2.98 \times 10^{-5} (\pm 2.03 \times 10^{-5})$	0.993(± 0.676)
-3.3	$1.84 \times 10^{-4} (\pm 1.07 \times 10^{-3})$	$2.11 \times 10^{-4} (\pm 1.06 \times 10^{-3})$	$2.70 \times 10^{-5} (\pm 2.13 \times 10^{-3})$	0.900(± 71.00)
-6.6	$1.59 \times 10^{-4} (\pm 1.27 \times 10^{-3})$	$1.76 \times 10^{-4} (\pm 1.27 \times 10^{-3})$	$1.70 \times 10^{-5} (\pm 2.54 \times 10^{-3})$	0.566(± 84.66)
	$\bar{\Theta}_0(\pm\bar{E}_{c0})$	$\bar{\Theta}_\tau(\pm\bar{E}_{c\tau})$	$\Delta\bar{\Theta}$	$\bar{K}_2(\pm\bar{E}_2)/0.0258$
6.6	$1.3971 \times 10^{-9} (\pm 4.41 \times 10^{-11})$	$1.3196 \times 10^{-9} (\pm 4.27 \times 10^{-11})$	$7.75 \times 10^{-11} (\pm 8.68 \times 10^{-11})$	1.001(± 2.891)
1.4	$4.3164 \times 10^{-9} (\pm 3.12 \times 10^{-10})$	$4.2391 \times 10^{-9} (\pm 2.94 \times 10^{-10})$	$7.73 \times 10^{-11} (\pm 6.06 \times 10^{-10})$	0.998(± 20.26)
-3.3	$1.66162 \times 10^{-8} (\pm 1.14 \times 10^{-9})$	$1.65396 \times 10^{-8} (\pm 1.13 \times 10^{-9})$	$7.66 \times 10^{-11} (\pm 2.27 \times 10^{-9})$	0.989(± 75.66)
-6.6	$6.27507 \times 10^{-8} (\pm 3.93 \times 10^{-9})$	$6.26751 \times 10^{-8} (\pm 3.95 \times 10^{-9})$	$7.56 \times 10^{-11} (\pm 7.88 \times 10^{-9})$	0.976(± 262.6)

the coupling strength τ increases. While results in the AWVA scheme indicate that the statistical errors of estimating \bar{K}_2 are independent of the coupling strength τ . Furthermore, if the experimental conditions permit multiple measurements, the measurements, where the central value deviates greatly from the theoretical value, can be eliminated to obtain the results with smaller error bars. In this case, the scheme with the WVA technique is superior to the scheme with the AWVA technique when the coupling strength $\tau > 1.5 \times 10^{-8}$ s. On the other hand, the advantage of the scheme with the VWVA technique is more obvious when the coupling strength is lower.

E. The measurements with different random seed

So far, the previous results and discussion have been based on the assumption that the thermal noise and shot noise of the detection may not cause the different series of noises detected on APD1 and APD2 in the AVVA scheme. Therefore, the shift $\Delta\Theta$ as well as sensitivity \bar{K}_2 were calculated from the dates of $\Theta(\tau = 0$ s) and $\Theta(\tau)$ with the same ξ . In other words, the noise is the same when you measure $\Theta(\tau = 0$ s) and $\Theta(\tau)$. Meanwhile, we calculated $\Delta(\delta t)$ from the dates of δt_0 and δt_τ with the same ξ . Note that these measurements can only be completed under special experimental conditions. Further, we use the dates with the different ξ to estimate the the shift $\Delta(\delta t)$ and $\Delta\Theta$. In particular, the results of the measurements with different random seed were calculated and were shown in Table. V. Where the average results $\delta\bar{t}_0(\pm\bar{E}_{t0})$, $\delta\bar{t}_\tau(\pm\bar{E}_{t\tau})$, $\bar{\Theta}_0(\pm\bar{E}_{c0})$ and $\bar{\Theta}_\tau(\pm\bar{E}_{c\tau})$ of multiple measurements are redefined:

$$\delta\bar{t}_0 = \sum_{i=1}^n \delta t_0(i)/n, \bar{E}_{t0} = \text{Max}\{|\delta\bar{t}_0 - \delta t_0(i)|\}, \quad (24)$$

$$\delta\bar{t}_\tau = \sum_{i=1}^n \delta t_\tau(i)/n, \bar{E}_{t\tau} = \text{Max}\{|\delta\bar{t}_\tau - \delta t_\tau(i)|\}, \quad (25)$$

$$\bar{\Theta}_0 = \sum_{i=1}^n \Theta_0(i)/n, \bar{E}_{c0} = \text{Max}\{|\bar{\Theta}_0 - \Theta_0(i)|\}, \quad (26)$$

$$\bar{\Theta}_\tau = \sum_{i=1}^n \Theta_\tau(i)/n, \bar{E}_{c\tau} = \text{Max}\{|\bar{\Theta}_\tau - \Theta_\tau(i)|\}, \quad (27)$$

where the (i) represents the result of the ith measurement with the different value of ξ , n represents the total number of measurements and n=7. Then, the corresponding shifts $\Delta(\delta\bar{t})$ and $\Delta\bar{\Theta}$ are obtained by the relationships $\Delta(\delta\bar{t}) = \delta\bar{t}_\tau - \delta\bar{t}_0$, $\Delta\bar{\Theta} = \bar{\Theta}_0 - \bar{\Theta}_\tau$. Furthermore, the sensitivity $\bar{K}_1(\pm\bar{E}_1)$ in scheme WVA and the sensitivity $\bar{K}_2(\pm\bar{E}_2)$ can be calculated by

$$\bar{K}_1 = \delta\bar{t}/\tau, \bar{E}_1 = (\bar{E}_{t0} + \bar{E}_{t\tau})/\tau, \quad (28)$$

$$\bar{K}_2 = \delta\bar{t}/\tau, \bar{E}_2 = (\bar{E}_{c0} + \bar{E}_{c\tau})/\tau. \quad (29)$$

Finally, we display these average results of the multiple measurements with different random seeds in Table. V. The simulation results show that the AWVA scheme has no advantage over the WVA scheme in the environment of weak noises with SNR= 6.6 dB and SNR= 1.4 dB. However, when multiple measurements are completed under strong noises with SNR= -3.3, the central value $\bar{K}_2/0.0258$ is closer to the theoretical value 1 and the values of statistical errors $\bar{E}_1/1.0 \times 10^3$ and $\bar{E}_2/0.0258$ are about the same. In addition, when multiple measurements are completed under strong noises with SNR= -6.6 dB, the AWVA scheme may have the potential to outperform the WVA scheme with a smaller deviation between the central value and the theoretical value. In general, the AWVA technique is a kind of efficient and brand-new scheme that can adapt to strong noise.

V. SUMMARY AND DISCUSSIONS

We have performed a new scheme with auto-correlative weak-value amplification for precision phase estimation. A stimulative experiment for estimating the time shift

with the standard weak-value amplification (WVA) technique and the auto-correlative weak-value amplification (AWVA) technique has been derived under Gaussian white noise with different signal-noise-ratio. In addition, a new quality (pointer), namely the auto-correlative intensity Θ , is defined in our scheme with the AWVA technique to estimate the small signal. Compared to fitting the shift of the Gaussian pointer with the standard WVA technique, measuring the shift of Θ has the advantage of suppressing noise, and the advantage of the scheme with the VWVA technique is more obvious when the SNR and the coupling strength are lower. Therefore, our results have demonstrated that the AWVA technique outperforms the standard WVA technique in the time domain even when the signal emerges in noise ($\text{SNR} < 0$). The robustness suggests that the AWVA technique can be applied for a vast range of weak measurements in the time domain.

Note that we assume that the contribution of all noise is Gaussian white noise in this paper. However, the real technique noise and environmental noise are far more complex than Gaussian white noise. In addition, many areas of physics have been replaced by colored noise (non-

Gaussian) [24–27]. Therefore, the auto-correlative weak-value amplification technique under the colored noises or the real noises will be investigated in our next work.

After completion of this work, we found that the AWVA technique can also be achieved on the weak measurement in the frequency domain. The quantity Θ can also be obtained by the integral of momentum mathematically, and how to realize this scheme will be our future study.

ACKNOWLEDGMENTS

This study is financially supported by the National Science Foundation of China (No. 41630317), MOST Special Fund from the State Key Laboratory of Geological Processes and Mineral Resources, China University of Geosciences (No. MSFGPMR01-4), the National Key Research and Development Program of China (Grant No. 2018YFC1503705), and the Fundamental Research Funds for the Central Universities of Ministry of Education of China (Grant No. G1323519204).

-
- [1] Y. Aharonov, D. Z. Albert, and L. Vaidman, How the result of a measurement of a component of the spin of a spin-1/2 particle can turn out to be 100, *Phys. Rev. Lett.* **60**, 1351 (1988).
 - [2] J. Dressel, M. Malik, F. M. Miatto, A. N. Jordan, and R. W. Boyd, Colloquium: Understanding quantum weak values: Basics and applications, *Rev. Mod. Phys.* **86**, 307 (2014).
 - [3] J. Ren, L. Qin, W. Feng, and X.-Q. Li, Weak-value-amplification analysis beyond the aharonov-albert-vaidman limit, *Phys. Rev. A* **102**, 042601 (2020).
 - [4] P. Yin, W.-H. Zhang, L. Xu, Z.-G. Liu, W.-F. Zhuang, L. Chen, M. Gong, Y. Ma, X.-X. Peng, G.-C. Li, J.-S. Xu, Z.-Q. Zhou, L. Zhang, G. Chen, C.-F. Li, and G.-C. Guo, Improving the precision of optical metrology by detecting fewer photons with biased weak measurement, *Light: Science & Applications* **10**, 103 (2021).
 - [5] F. Lecocq, L. Ranzani, G. A. Peterson, K. Cicak, X. Y. Jin, R. W. Simmonds, J. D. Teufel, and J. Aumentado, Efficient qubit measurement with a nonreciprocal microwave amplifier, *Phys. Rev. Lett.* **126**, 020502 (2021).
 - [6] C. Krafczyk, A. N. Jordan, M. E. Goggin, and P. G. Kwiat, Enhanced weak-value amplification via photon recycling, *Phys. Rev. Lett.* **126**, 220801 (2021).
 - [7] J. S. Lundeen and C. Bamber, Procedure for direct measurement of general quantum states using weak measurement, *Phys. Rev. Lett.* **108**, 070402 (2012).
 - [8] L. Xu, Z. Liu, A. Datta, G. C. Knee, J. S. Lundeen, Y.-q. Lu, and L. Zhang, Approaching quantum-limited metrology with imperfect detectors by using weak-value amplification, *Phys. Rev. Lett.* **125**, 080501 (2020).
 - [9] F.-Y. Ma, J.-G. Li, and J. Zou, The influence of non-gaussian noise on weak values, *Physics Letters A* **388**, 127027 (2021).
 - [10] N. Brunner and C. Simon, Measuring small longitudinal phase shifts: Weak measurements or standard interferometry?, *Phys. Rev. Lett.* **105**, 010405 (2010).
 - [11] G. I. Viza, J. Martínez-Rincón, G. A. Howland, H. Frostig, I. Shomroni, B. Dayan, and J. C. Howell, Weak-values technique for velocity measurements, *Opt. Lett.* **38**, 2949 (2013).
 - [12] Z. Li, L. Xie, Q. Ti, P. Duan, Z. Zhang, and C. Ren, Increasing the dynamic range of weak measurement with two pointers, *Phys. Rev. A* **102**, 023701 (2020).
 - [13] J.-H. Huang, F.-F. He, X.-Y. Duan, G.-J. Wang, and X.-Y. Hu, Modified weak-value-amplification technique for measuring a mirror's velocity based on the vernier effect, *Phys. Rev. A* **105**, 013718 (2022).
 - [14] P. B. Dixon, D. J. Starling, A. N. Jordan, and J. C. Howell, Ultrasensitive beam deflection measurement via interferometric weak value amplification, *Phys. Rev. Lett.* **102**, 173601 (2009).
 - [15] S. Kocsis, B. Braverman, S. Ravets, M. J. Stevens, R. P. Mirin, L. K. Shalm, and A. M. Steinberg, Observing the average trajectories of single photons in a two-slit interferometer, *Science* **332**, 1170 (2011).
 - [16] X.-Y. Xu, Y. Kedem, K. Sun, L. Vaidman, C.-F. Li, and G.-C. Guo, Phase estimation with weak measurement using a white light source, *Phys. Rev. Lett.* **111**, 033604 (2013).
 - [17] Y. Yang, Y. Xu, T. Guan, L. Shi, J. Li, D. Li, Y. He, X. Wang, Z. Li, and Y. Ji, Spectrum intensity ratio detection for frequency domain weak measurement system, *IEEE Photonics Journal* **12**, 1 (2020).
 - [18] B. de Lima Bernardo, S. Azevedo, and A. Rosas, Ultra-small polarization rotation measurements via weak value amplification, *Physics Letters A* **378**, 2029 (2014).
 - [19] O. S. Magaña Loaiza, M. Mirhosseini, B. Rodenburg,

- and R. W. Boyd, Amplification of angular rotations using weak measurements, *Phys. Rev. Lett.* **112**, 200401 (2014).
- [20] C. Ferrie and J. Combes, Weak value amplification is suboptimal for estimation and detection, *Phys. Rev. Lett.* **112**, 040406 (2014).
- [21] G. C. Knee and E. M. Gauger, When amplification with weak values fails to suppress technical noise, *Phys. Rev. X* **4**, 011032 (2014).
- [22] J. Zhu, Z. Li, Y. Liu, Y. Ye, Q. Ti, Z. Zhang, and F. Gao, Weak measurement with the peak-contrast-ratio pointer, *Phys. Rev. A* **103**, 032212 (2021).
- [23] H. Wu, P. Wu, Z.-C. Luo, L.-P. Xu, J.-H. Xie, T.-Y. Chang, H.-F. Shi, C.-L. Du, and H.-L. Cui, Pragmatic implementation with non-gaussian devices of noise-limited weak value amplification, *IEEE Photonics Journal* **13**, 1 (2021).
- [24] R. F. Fox, I. R. Gatland, R. Roy, and G. Vemuri, Fast, accurate algorithm for numerical simulation of exponentially correlated colored noise, *Phys. Rev. A* **38**, 5938 (1988).
- [25] B. L. Hu, J. P. Paz, and Y. Zhang, Quantum brownian motion in a general environment: Exact master equation with nonlocal dissipation and colored noise, *Phys. Rev. D* **45**, 2843 (1992).
- [26] J.-L. Wu, W.-L. Duan, Y. Luo, and F. Yang, Time delay and non-gaussian noise-enhanced stability of foraging colony system, *Physica A: Statistical Mechanics and its Applications* **553**, 124253 (2020).
- [27] O. V. Pountounigni, R. Yamapi, C. Tchawoua, V. Pierro, and G. Filatrella, Detection of signals in presence of noise through josephson junction switching currents, *Phys. Rev. E* **101**, 052205 (2020).
- [28] M. Parikh, F. Wilczek, and G. Zahariade, Signatures of the quantization of gravity at gravitational wave detectors, *Phys. Rev. D* **104**, 046021 (2021).
- [29] A. Feizpour, X. Xing, and A. M. Steinberg, Amplifying single-photon nonlinearity using weak measurements, *Phys. Rev. Lett.* **107**, 133603 (2011).
- [30] Y. Kedem, Using technical noise to increase the signal-to-noise ratio of measurements via imaginary weak values, *Phys. Rev. A* **85**, 060102 (2012).
- [31] A. N. Jordan, J. Martínez-Rincón, and J. C. Howell, Technical advantages for weak-value amplification: When less is more, *Phys. Rev. X* **4**, 011031 (2014).
- [32] J. Harris, R. W. Boyd, and J. S. Lundeen, Weak value amplification can outperform conventional measurement in the presence of detector saturation, *Phys. Rev. Lett.* **118**, 070802 (2017).
- [33] A. Nishizawa, K. Nakamura, and M.-K. Fujimoto, Weak-value amplification in a shot-noise-limited interferometer, *Phys. Rev. A* **85**, 062108 (2012).
- [34] D. Li, T. Guan, Y. He, F. Liu, A. Yang, Q. He, Z. Shen, and M. Xin, A chiral sensor based on weak measurement for the determination of proline enantiomers in diverse measuring circumstances, *Biosensors and Bioelectronics* **110**, 103 (2018).
- [35] X. Zhou, W. Cheng, S. Liu, J. Zhang, C. Yang, and Z. Luo, Tunable and high-sensitivity temperature-sensing method based on weak-value amplification of goos-hänchen shifts in a graphene-coated system, *Optics Communications* **483**, 126655 (2021).
- [36] T. Guan, Y. Yang, Q. Zhang, Y. He, N. Xu, D. Li, L. Shi, Y. Xu, and X. Wang, Label-free and Non-destruction Determination of Single- and Double-Strand DNA based on Quantum Weak Measurement, *Scientific Reports* **9**, 1891 (2019).
- [37] X. Zhu and Y.-X. Zhang, Influence of environmental noise on the weak value amplification, *Quantum Information Processing* **15**, 3421 (2016).
- [38] J. Sinclair, M. Hallaji, A. M. Steinberg, J. Tollaksen, and A. N. Jordan, Weak-value amplification and optimal parameter estimation in the presence of correlated noise, *Phys. Rev. A* **96**, 052128 (2017).
- [39] Y. Lee, T. Cheatham, and J. Wiesner, Application of correlation analysis to the detection of periodic signals in noise, *Proceedings of the IRE* **38**, 1165 (1950).
- [40] Y. Liu, J. Liu, and R. Kennel, Frequency measurement method of signals with low signal-to-noise-ratio using cross-correlation, *Machines* **9**, 10.3390/machines9060123 (2021).
- [41] E. J. Takahashi, P. Lan, O. D. Mücke, Y. Nabekawa, and K. Midorikawa, Attosecond nonlinear optics using gigawatt-scale isolated attosecond pulses, *Nature Communications* **4**, 2691 (2013).
- [42] R. Jozsa, Complex weak values in quantum measurement, *Phys. Rev. A* **76**, 044103 (2007).
- [43] Y. Susa, Y. Shikano, and A. Hosoya, Optimal probe wave function of weak-value amplification, *Phys. Rev. A* **85**, 052110 (2012).